

Article

# Molecular Dynamics Simulation of the Incident Energy Effect on the Properties of TiN Films

Jiao Li <sup>1</sup>, Jun Lin <sup>2,\*</sup>, Qingyuan Ma <sup>2</sup>, Hanxiao Luan <sup>2</sup>, Lihua Zhu <sup>3</sup>, Ruqing Bai <sup>4,\*</sup>, Guiwei Dong <sup>2</sup>, Diangang Wang <sup>2</sup>, Yanjin Guan <sup>2</sup> and Xiaocui Zhang <sup>5</sup>

<sup>1</sup> School of Mechanical and Electronic Engineering, Shandong Jianzhu University, Jinan 250101, China

<sup>2</sup> Key Laboratory for Liquid-Solid Structural Evolution & Processing of Materials (Ministry of Education), Shandong University, Jinan 250061, China

<sup>3</sup> School of Mechanical Engineering, Shandong University of Technology, Zibo 255000, China

<sup>4</sup> State Key Laboratory of Mechanical Transmission, Chongqing University, Chongqing 400044, China

<sup>5</sup> Tianjin Product Quality Inspection Technology Research Institute, Tianjin 300384, China

\* Correspondence: linjun@sdu.edu.cn (J.L.); ruqing.bai@cqu.edu.cn (R.B.)

**Abstract:** In this work, to investigate the physical vapor deposition (PVD)-deposited TiN coating on the TiN(001) substrate, the process was simulated using the molecular dynamics (MD) method with the 2NN-MEAM (nearest-neighbor modified embedded atom method) potential. The results revealed that the growth mode of TiN film is determined by incident energy. When the incident energy is low, the deposited atoms have weak mobility after momentum transfer with the substrate and cannot fill the vacancy in the TiN film, and thus the TiN film eventually grows in an island shape. When increasing the incident energy, the vibration of atoms on the deposited surface is intensified, and some atoms on the film surface jump. Therefore, the non-thermal diffusion occurs, resulting in defect reduction on the TiN film and forming a lamellar growth with a more continuous and complete film. The growing incident energy continuously reduces the surface roughness of the TiN film.

**Keywords:** molecular dynamics; TiN; atomic deposition; incident energy; film performance



**Citation:** Li, J.; Lin, J.; Ma, Q.; Luan, H.; Zhu, L.; Bai, R.; Dong, G.; Wang, D.; Guan, Y.; Zhang, X. Molecular Dynamics Simulation of the Incident Energy Effect on the Properties of TiN Films. *Coatings* **2023**, *13*, 794. <https://doi.org/10.3390/coatings13040794>

Academic Editor: Bohayra Mortazavi

Received: 29 March 2023

Revised: 10 April 2023

Accepted: 14 April 2023

Published: 19 April 2023



**Copyright:** © 2023 by the authors. Licensee MDPI, Basel, Switzerland. This article is an open access article distributed under the terms and conditions of the Creative Commons Attribution (CC BY) license (<https://creativecommons.org/licenses/by/4.0/>).

## 1. Introduction

Titanium nitride (TiN) of face-centered cubic structure possesses good thermal stability, high wear protection, and corrosion and oxidation resistance [1–3], which is often deposited on the die steel surface as a coating material by physical vapor deposition (PVD) to effectively improve the surface hardness, wear resistance, and service life of the die steel [4,5]. To reduce the residual stress and improve the mechanical properties of the film, it is of great significance to study the interaction between deposited particles and substrate on an atomic scale and reveal the deposition behavior of the film at the initial growth stage, which can be used to adjust the production process and improve the production quality of the film.

Limited by current experimental instruments, there are few studies on the microstructure growth and deposition mechanism of TiN thin films [6]. With the development of computer theory and technology, the molecular dynamics method has been applied more and more to simulate the interaction between atoms and molecules in various systems [7–9]. The micro-information, such as kinetic energy, potential energy, and the interactions of particles, can be extracted from the simulation results, which are hardly provided by the existing experimental conditions.

The performance of the deposited film is determined by various PVD conditions, among which the incident energy of deposited particles is a major one. Under the impact energy of the charged particles, some of the target atoms will leave the target after gaining energy and become incident atoms, which carry a certain amount of incident energy and may move to the base. By simulating the deposition process of TiN film, Xu et al. [10]

found that the reflection number of N atoms increased significantly with the increase of incident energy, and sputtering appeared when the incident energy of atoms increased to 6 eV. The deposition efficiency of Ti atoms is close to 100% when the incident energy is 0.5–10 eV. Zheng et al. [11] performed MD analysis on the deposition process of Al atoms on Cu(001) under different incident energies. The result showed that increasing the initial incident energy of deposited particles can significantly reduce the surface roughness of an Al film on a Cu(001) substrate. Hwang et al. [12] studied the deposition of Cu clusters on a Si substrate, and found that the film surface roughness was the lowest when the incident energy was 15 eV. With the increase of incident energy, the energy exchange frequency between deposited atoms increases, and the biaxial stress decreases. When the incident energy is greater than 40 eV, large-scale sputtering occurs. The deposition of Fe and Co on Cu substrate was investigated by Hong et al. [13]. The average stress of the deposition layer and the base layer alternated from compressive stress to tensile stress when the incident energy increased from 1 eV to 5 eV due to the influence of island aggregation in the film-forming process. Regardless of the incident energy, the surface roughness of the Fe–Cu system is better than that of the Co–Cu system, and the interfacial atom mixing degree of the Fe–Cu system is lower.

In order to reveal the particle deposition behavior and microscopic growth process of TiN film in the PVD process, this paper established a TiN deposition model based on molecular dynamics simulation. The effects of different incident energies on film coverage, surface quality, density, and film stress were investigated.

## 2. Simulation Method

### 2.1. Model and Potential

The interatomic potential is a key element that is significant for predicting structural properties and determines the feasibility and reliability of the MD modeling. The second nearest-neighbor modified embedded-atom method (2NN MEAM) considers the directivity of bonds and the interaction between the 2NN atoms. Therefore, it is suitable to describe the atomic deposition process. The 2NN MEAM potential parameters for the Ti, N, and Ti–N binary systems are taken from Kim et al. [14] and Xu et al. [15].

Atomic simulation was carried out by using the parallel MD code LAMMPS. The three-dimensional model of the simulation box is indicated in Figure 1. The blue atom represents Ti, and the yellow atom indicates N. The entire substrate is composed of TiN(001), where the  $x$ ,  $y$ , and  $z$  directions correspond to the crystal directions of [0,0,1], [0,1,0], and [0,0,1], respectively, with dimensions of  $16 a_{\text{TiN}} \times 16 a_{\text{TiN}} \times 6 a_{\text{TiN}}$  ( $a_{\text{TiN}}$  is the TiN lattice constant, values 4.264 Å). The boundary conditions are set as p p f, that is, the  $x$  and  $y$  directions are periodic boundary conditions, and the  $z$  direction is a fixed boundary condition, so the matrix can be regarded as an infinite plate on the  $x$ - $y$  plane. The bottom two layers of atoms are fixed layers to avoid interaction between incident atoms and the matrix, resulting in momentum transfer and eventual migration of the whole system. In addition to the fixed layer, the other atoms in the matrix are isothermal layers controlled by an NVT ensemble. The substrate temperature was initially set at 700 K [16], and the substrate atomic velocity was corrected every ten time steps to ensure a constant temperature for TiN film growth.

The distance between the incident layer and the surface layer is 20 Å. According to different deposition parameters, an equal number of N and Ti atoms are emitted to the substrate at random locations in the incident layer. In order to level up the deposition efficiency and avoid the invalid simulation, a virtual wall is found at the upper part of the simulation box. If the incident atom is reflected after hitting the base, the normal velocity component will reverse as  $-v_z$  after hitting the virtual wall in the reflection process, and other velocity components will remain unchanged, making it continue depositing. A total of  $32 \times 32 \times 32 = 32,768$  atoms were deposited. In this simulation, four different incident energies were considered in magnetron sputtering [17,18], which were 0.1 eV, 1 eV, 4 eV, and 10 eV, respectively. The visualization of the model was realized by OVITO.

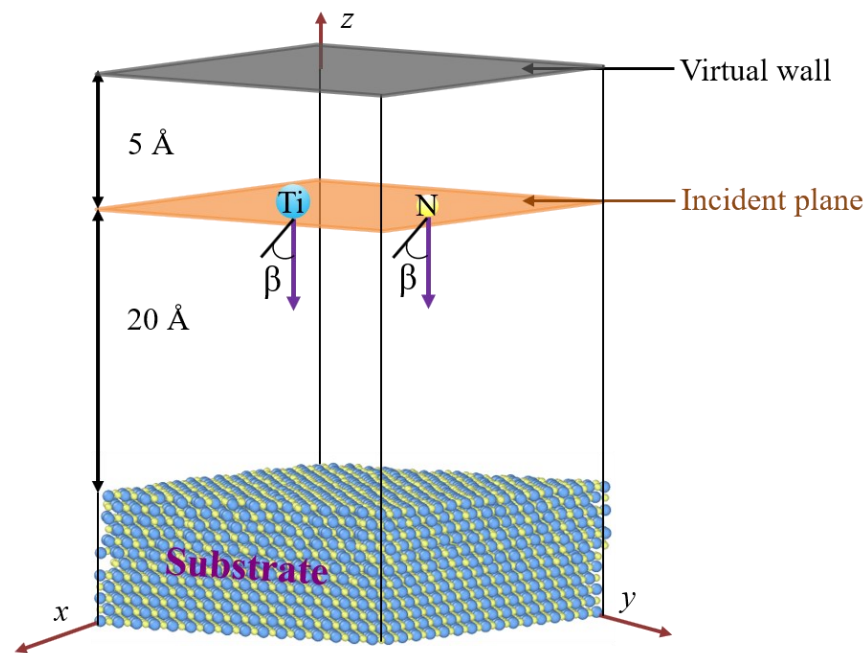


**Figure 1.** MD simulation box for TiN film deposition.

## 2.2. Calculation and Analysis Method

Surface roughness is commonly used to describe the surface quality of the thin film. In general, the smaller the surface roughness is, the better the wear resistance and oxidation resistance of the film can be obtained. In this molecular dynamics simulation, the surface roughness of the film can be calculated from the  $z$  coordinates of the atoms on the film surface, which can be expressed by the root mean square (RMS) roughness  $R_q$ .

$$R_q = \sqrt{\frac{\sum_{i=1}^N (z_i - \bar{z})^2}{N}} \quad (1)$$

where  $i$  denotes the surface atom on the film,  $N$  represents the number of atoms exposed on the surface,  $z_i$  means the height of atoms on the surface, and  $\bar{z}$  is the average height of all surface atoms.

The layer coverage function at the interface reflects the intermixing of incident atoms and base atoms on the deposition surface, and it can also characterize the bonding properties of the film. Layer coverage function  $\gamma$  can be defined as:

$$\gamma = \frac{n}{M} \quad (2)$$

where  $n$  represents the number of Ti and N atoms deposited in the layer, and  $M$  represents the total number of atoms contained in the layer.

In order to study the stress variation trend of deposited Ti and N atoms during the growth of TiN film, the average stress  $\sigma_{ab}^{avg}$  of each atom in TiN film is defined as:

$$\sigma_{ab}^{avg} = \frac{1}{L} \sum_{j=1}^L \sigma_{ab}^j \quad (3)$$

where  $\sigma_{ab}^j$  represents the stress tensor of the  $j$ th atom at the layer,  $a$  and  $b$  are the stress tensor indices, and  $L$  indicates the number of atoms at this layer.

Due to the influence of the growth environment and production process, as well as the properties of its own materials, the residual stress of the TiN film has two sides. On the one hand, the residual compressive stress can improve the mechanical properties of

TiN film to a certain extent. On the other hand, when the residual stress is too large, it will seriously affect the fracture toughness of the film. Since the shear stress is one order of magnitude lower than the normal stress in the case of deposition [19], the average biaxial stress  $(\sigma_{xx}^{avg} + \sigma_{yy}^{avg})/2$  of TiN film is often taken into account and applied to characterize the residual stress of the layer.

### 3. Results and Discussion

#### 3.1. Surface Quality

The surface morphologies of the TiN film at the end of the MD simulation are presented in Figure 2, with the incident energies of 0.1 eV, 1 eV, 4 eV, and 10 eV, respectively.

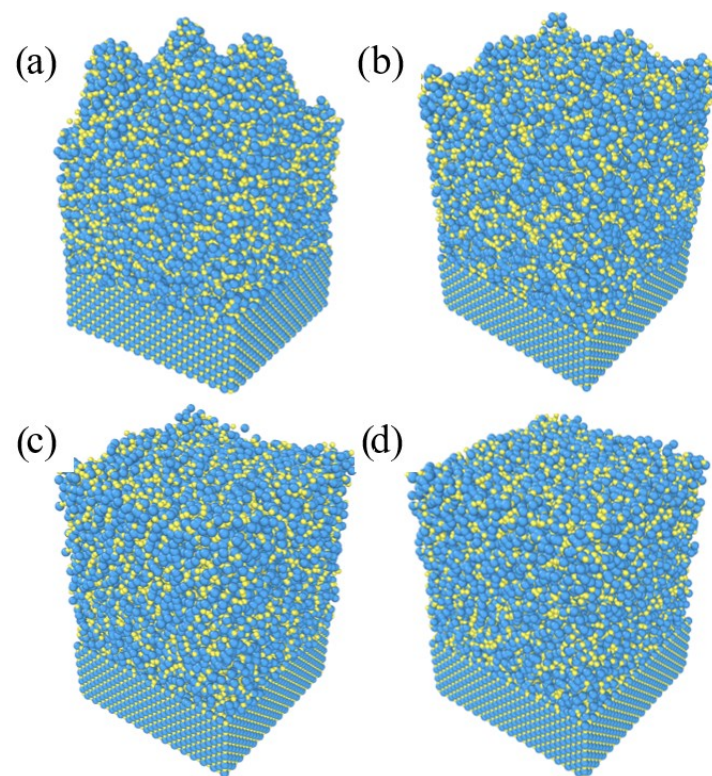


**Figure 2.** Atomic configurations of the TiN film at different incident energies. (a) 0.1 eV; (b) 1 eV; (c) 4 eV; (d) 10 eV.

The film configuration of the material deposited at the incident energy of 0.1 eV is shown in Figure 2a. It can be observed that the film has obvious island deposition, resulting in a rough surface and poor film quality due to the low mobility of the incident atoms. Before reaching the base, the injection atom is easy to gather and nucleate with the nearby deposited atoms, forming several small clusters. The spacing between small clusters is large, and TiN film grows in an island shape. In addition, atoms with low incident energy have a poor ability to fill vacancies, resulting in many gullies between islands and a large number of gaps and vacancies in the film.

When the incident energy exceeds 1 eV, the latent heat of condensation is released, and part of the adatom's kinetic energy is transferred to the surface atoms during the interaction between the deposited and the surface atoms. These powers exacerbate the thermal vibration of the sedimentary surface atoms and make some surface atoms bounce, forming the thermal diffusion and reducing the space between the islands. Finally, a continuous film with a smooth surface is generated, as shown in Figure 2b–d. Therefore, the thin films are gradually thickened in a lamellar growth way instead of the island growth mode in cases of low incident energy.

By substituting the  $z$  coordinates of the surface atoms into Equation (1), the RMS roughness of the film surface can be obtained, which is listed in Table 1.

**Table 1.**  $R_q$  of the film surface at different incident energies.

Incident energy (eV)	0.1	1	4	10
RMS roughness ( $\text{\AA}$ )	18.27	7.03	6.89	5.97

As can be seen from Figure 2 and Table 1, when the energy of incident atoms Ti and N is low, the island deposition phenomenon of TiN films is serious. With the increase of incident energy, the island growth effect is weakened and the film grows in layers. When the incident energy is 0.1 eV, the film surface is relatively rough, with an RMS roughness of 18.27  $\text{\AA}$ . As the incident energy goes to 1 eV, the roughness of the film becomes 7.03  $\text{\AA}$ , with a significant decrease of 61.52%. The surface roughness continues to decrease with the growing incident energy. However, the decrease rate reduces. When the incident energy reaches 10 eV, the roughness descends to 5.97  $\text{\AA}$ , which is 15.08% lower than that at 1 eV.

To deeply investigate the overall morphology of the thin film, the surface topography fluctuations are reflected by liner root mean square roughness. The film was cut apart at 0.5  $a_{\text{TiN}}$  intervals along the  $x$  direction of the film to obtain 32 sections, and the linear root mean square roughness was calculated and depicted in Figure 3.

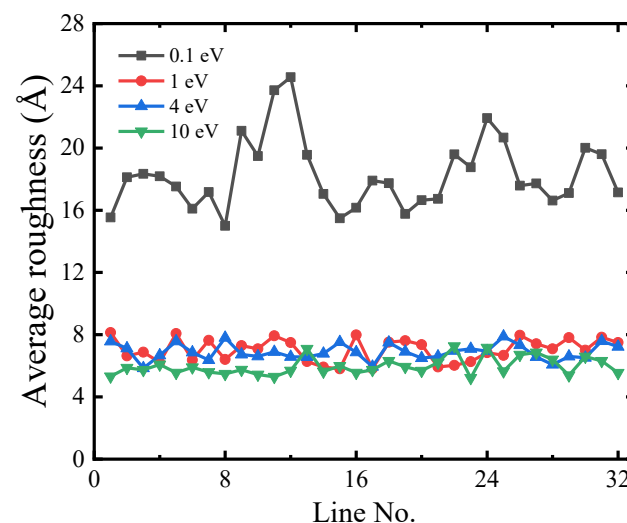


**Figure 3.** Effect of different incident energies on the line RMS roughness of the TiN thin film.

When the incident energy is 0.1 eV, the film grows in an island shape, resulting in large surface topography fluctuations, large RMS roughness values, and large oscillation amplitudes. The maximum RMS roughness is 24.55  $\text{\AA}$  and the minimum is 15.01  $\text{\AA}$ , meaning it oscillates with an amplitude of 9.54  $\text{\AA}$ . With aggrandizing the incident energy, the film grows to be lamellar, the root mean square roughness becomes smaller, and the fluctuations decrease to 1.78  $\text{\AA}$ , with 81.3% smoother than that of 0.1 eV. The oscillation of the simulated surface roughness is also consistent with the simulation results of Chu et al. [20]. When the thin film grows in layers, the surface roughness of the Fe deposited on the Cu(001) substrate also shows an oscillation of 0.6–1.0  $\text{\AA}$ .

### 3.2. Interface Mixing

In order to study the intermixing phenomenon, the layer coverage function expressed in Equation (2) was introduced to describe the ratio between the numbers of a type of atom and all layer atoms. Figure 4 gives the layer coverage ratio of deposited atoms at the TiN(001) substrate interface under different incident energies, where layer 0 represents the



upper surface interface of the TiN(001) base. The positive and negative indices denote the sedimentary layers above the interface and the substrate layers below the interface.

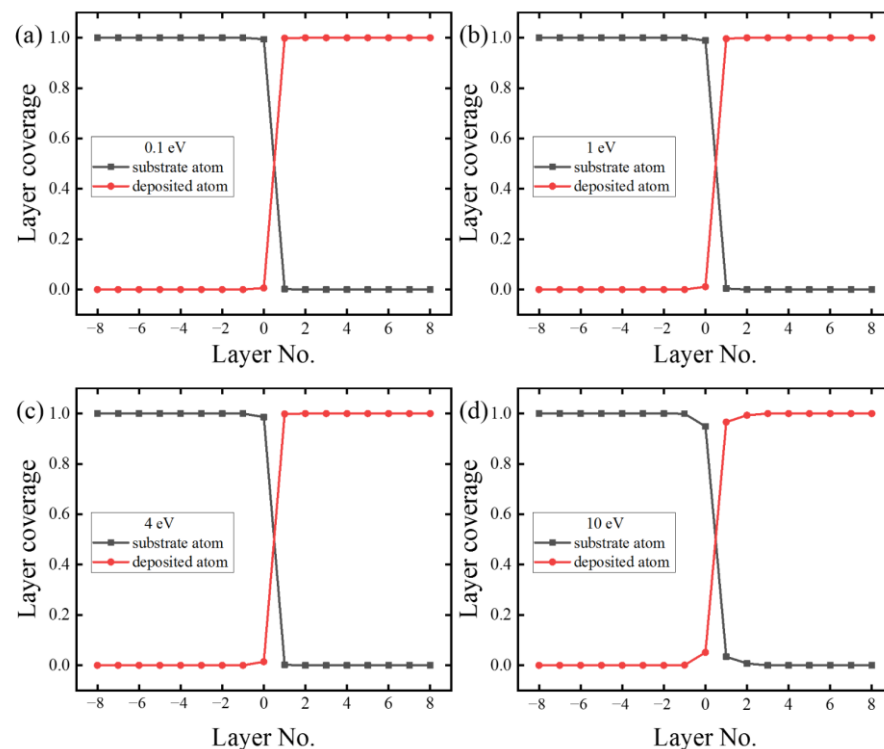


**Figure 4.** Layer coverage ratio of the TiN film at different incident energies. (a) 0.1 eV; (b) 1 eV; (c) 4 eV; (d) 10 eV.

As can be seen from Figure 4, the phenomenon of atomic penetration and atomic exchange at the basement surface is quite limited, similar to that of binary systems such as Cu–Fe [21] and Co–Al [22]. When the incident energy of the Ti and N atoms increases from 0.1 eV to 10 eV, the layer coverage function of the deposited atoms on the substrate surface increases from 0.6% to 5.1%. The layer coverage functions of the 1st and 2nd layers no longer remain 0 and 1, when the incident energy is 10 eV. This phenomenon signifies the active interpenetration between a small amount of deposit and basal surface atoms. When the deposited atom has excessive power, it may interact and destroy the chemical bonds between Ti and N atoms in the basement and then mix with the substrate. Meanwhile, it is also found that a few base atoms are bombarded during the deposition process, resulting in sputtering behavior and movement towards the deposition layer.

### 3.3. Internal Stress

The average mean biaxial stress computed using Equation (3) is shown in Figure 5 to explore the residual stress of TiN film on the substrate. Herein, the positive and negative stresses refer to compressive and tensile stress, meaning that the repulsion and attraction forces are borne, respectively.

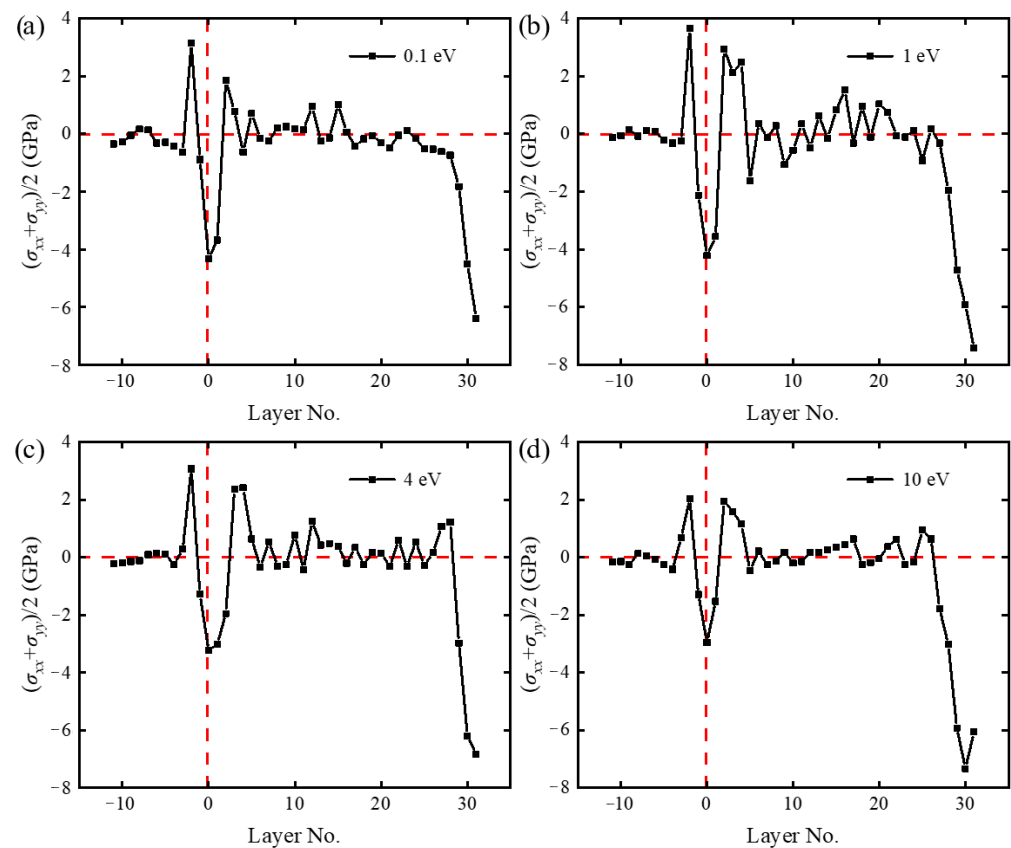


**Figure 5.** Biaxial stress of TiN thin films at different incident energies. (a) 0.1 eV; (b) 1 eV; (c) 4 eV; (d) 10 eV.

It can be seen from Figure 5 that the average mean biaxial stress in the substrate is close to 0, with a relatively small fluctuation, demonstrating that the lattice structures remain well in the deposition process. The compressive stress occurs underlying the substrate surface (−2nd) due to the shot-peening effect of energetically deposited atoms. This stress suddenly turns to tensile at the interface. This may be caused by the fact that there is a mismatch between the substrate and the coating [23], since the absorption ability of the incident N and Ti atoms is not identical [10]. When the incident energy increases, the compression and tension peak values reduce, benefiting from the increasing diffusing of adatoms and intermixing, as analyzed in the last section [19]. With the deposition proceeding, the stress converts to compressive and then gradually reduces and oscillates with a small positive average stress. The small stress in the coating is the result of a relatively ordered arrangement with lamellar growth mode, and the fluctuation is caused by the film growth at high temperature and the formation of holes. On the film surface, the attractive force is generated due to the incomplete atomic bond constraint. As shown in Figure 2, the upper atoms cannot remain structurally coherent with the underlying lattice and thus undergo an attraction force from the lower layer [24,25].

#### 4. Conclusions

A large-scale MD model was constructed to simulate the TiN deposition process on a TiN (001) basement. By analyzing the morphology, surface roughness, layer coverage function, and biaxial stress of TiN films, the effects of different incident energies on the deposition behavior and properties of TiN films were studied.

- (1) The growth mode of TiN film is mainly determined by the incident energy. When the incident energy is low, TiN thin films grow as islands. When the incident energy is increased, the tin films grow in layers;

- (2) With the increase of incident energy from deposited Ti and N atoms, the roughness of TiN films decreases, and the oscillation amplitude of line roughness decreases;
- (3) The coverage of the middle layer is basically unchanged and is not affected by the incident energy, which is consistent with many binary alloy experiments;
- (4) With increasing incident energy, a compressive stress existed underlying the substrate-film interface due to the atom peening. The interface presents the attraction force caused by the lattice mismatch between the ordered substrate and the initially island-grown coatings. The tensile force of the atoms on the film surface is exerted by the internal, structurally arranged atoms.

As part of the future scope of the work, the authors will delve deeper into the energy transport pathway and the atom arrangement, which help to recognize the microstructure of the deposition film.

**Author Contributions:** Conceptualization, J.L. (Jun Lin); methodology, Q.M.; software, Q.M. and H.L.; validation, J.L. (Jiao Li) and R.B.; formal analysis, L.Z. and X.Z.; investigation, Y.G.; resources, G.D. and D.W.; data curation, L.Z.; writing—original draft preparation, Q.M.; writing—review and editing, J.L. (Jiao Li); visualization, Q.M. and J.L. (Jiao Li); supervision, Y.G. All authors have read and agreed to the published version of the manuscript.

**Funding:** This project is supported by the National Key Research and Development Program of China (2020YFB2010300), the National Natural Science Foundation of China (52005299), and the Shandong Provincial Natural Science Foundation (ZR2020QE169).

**Institutional Review Board Statement:** Not applicable.

**Informed Consent Statement:** Not applicable.

**Data Availability Statement:** The data are not publicly available due to privacy.

**Conflicts of Interest:** The authors declare no conflict of interest.

## References

1. Vega, J.; Scheerer, H.; Andersohn, G.; Oechsner, M. Experimental studies of the effect of Ti interlayers on the corrosion resistance of TiN PVD coatings by using electrochemical methods. *Corros. Sci.* **2018**, *133*, 240–250. [\[CrossRef\]](#)
2. Das, S.; Guha, S.; Ghadai, R.; Sharma, A. Influence of nitrogen gas over microstructural, vibrational and mechanical properties of CVD Titanium Nitride (TiN) thin film coating. *Ceram. Int.* **2021**, *47*, 16809–16819. [\[CrossRef\]](#)
3. Lang, F.; Yu, Z. The corrosion resistance and wear resistance of thick TiN coatings deposited by arc ion plating. *Surf. Coat. Technol.* **2001**, *145*, 80–87. [\[CrossRef\]](#)
4. Malvajerdi, S.S.; Malvajerdi, A.S.; Ghanaatshoar, M. Protection of CK45 carbon steel tillage tools using TiN coating deposited by an arc-PVD method. *Ceram. Int.* **2019**, *45*, 3816–3822. [\[CrossRef\]](#)
5. Liu, C.; Bi, Q. A Matthews. EIS comparison on corrosion performance of PVD TiN and CrN coated mild steel in 0.5 N NaCl aqueous solution. *Corros. Sci.* **2001**, *43*, 1953–1961. [\[CrossRef\]](#)
6. Krella, A. Resistance of PVD coatings to erosive and wear processes: A review. *Coatings* **2020**, *10*, 921. [\[CrossRef\]](#)
7. Robustelli, P.; Piana, S.; Shaw, D.E. Developing a molecular dynamics force field for both folded and disordered protein states. *Proc. Natl. Acad. Sci. USA* **2018**, *115*, 4758–4766. [\[CrossRef\]](#)
8. Jiang, Z.; You, L.; Dou, W.; Sun, T.; Xu, P. Effects of an electric field on the conformational transition of the protein: A molecular dynamics simulation study. *Polymers* **2019**, *11*, 282. [\[CrossRef\]](#)
9. Gao, P.; Huang, Z.; Yu, H. Exploration of the dehydrogenation pathways of ammonia diborane and diammoniate of diborane by molecular dynamics simulations using reactive force fields. *J. Phys. Chem. A* **2020**, *124*, 1698–1704. [\[CrossRef\]](#)
10. Xu, Z.; Zeng, Q.; Yuan, L.; Qin, Y.; Chen, M.; Shan, D. Molecular dynamics study of the interactions of incident N or Ti atoms with the tin (001) surface. *Appl. Surf. Sci.* **2016**, *360*, 946–952. [\[CrossRef\]](#)
11. Hong, Z.H.; Hwang, S.F.; Fang, T.H. Atomic-level stress calculation and surface roughness of film deposition process using molecular dynamics simulation. *Comput. Mater. Sci.* **2010**, *48*, 520–528. [\[CrossRef\]](#)
12. Hwang, S.F.; Li, Y.H.; Hong, Z.H. Molecular dynamic simulation for Cu cluster deposition on Si substrate. *Comput. Mater. Sci.* **2012**, *56*, 85–94. [\[CrossRef\]](#)
13. Hong, Z.H.; Hwang, S.F.; Fang, T.H. The deposition of Fe or Co clusters on Cu substrate by molecular dynamic simulation. *Surf. Sci.* **2011**, *605*, 46–53. [\[CrossRef\]](#)
14. Kim, Y.M.; Lee, B.J. Modified embedded-atom method interatomic potentials for the Ti–C and Ti–N binary systems. *Acta Mater.* **2008**, *56*, 3481–3489. [\[CrossRef\]](#)



15. Xu, Z.; Yuan, L.; Shan, D.; Guo, B. A molecular dynamics simulation of TiN film growth on TiN (0 0 1). *Comput. Mater. Sci.* **2011**, *50*, 1432–1436. [[CrossRef](#)]
16. Panjan, P.; Drnovšek, A.; Terek, P.; Miletić, A.; Čekada, M.; Panjan, M. Comparative study of tribological behavior of TiN hard coatings deposited by various pvd deposition techniques. *Coatings* **2022**, *12*, 294. [[CrossRef](#)]
17. Greczynski, G.; Mraz, S.; Schneider, J.M.; Hultman, L. Metal-ion subplantation: A game changer for controlling nanostructure and phase formation during film growth by physical vapor deposition. *J. Appl. Phys.* **2020**, *127*, 180901. [[CrossRef](#)]
18. Lu, T.M.; Zhao, Y.P.; Drotar, J.T.; Karabacak, T.; Wang, G.C. Novel mechanisms on the growth morphology of films. *MRS Proc.* **2002**, *749*, 1–6. [[CrossRef](#)]
19. Amini, H.; Gholizadeh, P.; Poursaeidi, E.; Davoodi, J. A molecular dynamics simulation of Ti–TiN multilayer deposition on FeCrNi (001) alloy substrate. *Vacuum* **2021**, *193*, 110519. [[CrossRef](#)]
20. Chu, C.J.; Chen, T.C. Surface properties of film deposition using molecular dynamics simulation. *Surf. Coat. Technol.* **2006**, *201*, 1796–1804. [[CrossRef](#)]
21. Lee, S.G.; Chung, Y.C. Molecular-dynamics investigation of the surface characteristics of Fe–Cu magnetic thin-film layers. *J. Vac. Sci. Technol. A* **2008**, *26*, 1392–1396. [[CrossRef](#)]
22. Kim, S.P.; Lee, S.C.; Lee, K.R.; Chung, Y.C. Asymmetric surface intermixing during thin-film growth in the Co–Al system: Role of local acceleration of the deposited atoms. *Acta Mater.* **2008**, *56*, 1011–1017. [[CrossRef](#)]
23. Xi, Y.; Bai, Y.; Gao, K.; Pang, X.; Yang, H.; Yan, L.; Volinsky, A.A. Residual stress and microstructure effects on mechanical, tribological and electrical properties of TiN coatings on 304 stainless steel. *Ceram. Int.* **2018**, *44*, 15851–15858. [[CrossRef](#)]
24. Zhu, G.; Sun, J.; Zhang, L.; Gan, Z. Molecular dynamics simulation of temperature effects on deposition of Cu film on Si by magnetron sputtering. *J. Cryst. Growth* **2018**, *492*, 60–66. [[CrossRef](#)]
25. Cammarata, R.C. Surface and interface stress effects in thin films. *Prog. Surf. Sci.* **1994**, *46*, 1–38. [[CrossRef](#)]

**Disclaimer/Publisher’s Note:** The statements, opinions and data contained in all publications are solely those of the individual author(s) and contributor(s) and not of MDPI and/or the editor(s). MDPI and/or the editor(s) disclaim responsibility for any injury to people or property resulting from any ideas, methods, instructions or products referred to in the content.